INORGANIC CHEMISTRY FRONTIERS

RESEARCH ARTICLE

View Article Online
View Journal | View Issue

Cite this: *Inorg. Chem. Front.*, 2026, **13**, 963

A high-performance IR nonlinear optical material $Sr_3MnGe_2S_8$ achieved *via* partial cation substitution-induced structural transformation

A-Lan Xu,[a,b,c] Mao-Yin Ran, *[b,d] Zuju Ma,[e] Xin-Tao Wu, [b] Hua Lin *[a,b] and Qi-Long Zhu *[a,b]

The development of Mn-based infrared nonlinear optical (IR-NLO) materials that concurrently exhibit a large second-harmonic generation response (SHG > 1.0 × $AgGaS_2$) and a wide band gap (E_g > 3.0 eV) remains a formidable challenge. Herein, we demonstrate a partial cation substitution strategy to address this issue, successfully transforming centrosymmetric Sr_2GeS_4 into a novel non-centrosymmetric quaternary sulfide, $Sr_3MnGe_2S_8$. The compound features a three-dimensional framework constructed from corner-sharing [MnS_4] and [GeS_4] tetrahedra, with Sr^{2+} cations residing in the interstitial spaces. $Sr_3MnGe_2S_8$ achieves an outstanding balance of key IR-NLO properties: it shows a strong SHG response (2.4 × $AgGaS_2$ at 2050 nm), a high laser-induced damage threshold (13.4 × $AgGaS_2$), and a wide E_g of 3.06 eV—ranking it among the best-performing Mn-based chalcogenides. Theoretical calculations and structural analysis reveal that the excellent NLO performance originates from the synergistic effects between the two distinct types of functional units. This work provides a valuable paradigm for designing high-performance IR-NLO materials through rational structural transformation, highlighting the power of chemical substitution in overcoming property trade-offs.

Received 28th October 2025,
Accepted 14th November 2025

DOI: 10.1039/d5qi02182k

rsc.li/frontiers-inorganic

Introduction

Nonlinear optical (NLO) crystals serve as the cornerstone materials for laser frequency conversion and play a pivotal role in a variety of applications, including environmental monitoring, medical imaging, infrared (IR) remote sensing, and national defense and security.[1] Currently, commercially available NLO crystals operating in the mid- to far-IR region—such as $AgGaS_2$, $AgGaSe_2$, and $ZnGeP_2$—suffer from intrinsic limitations, notably a narrow bandgap (E_g), which leads to a low laser-induced damage threshold (LIDT) and undesirable two-photon absorption (TPA).[2] These drawbacks significantly restrict their application in high-power infrared laser systems. Consequently, there is an urgent need to explore and synthesize new IR-NLO crystals that exhibit superior overall performance, particularly those possessing both a wide E_g and a large second-harmonic generation (SHG) response.[3]

Transition metal-based chalcogenides have garnered significant attention as a compelling class of materials for IR-NLO applications, distinguished by their structurally tunable frameworks, adaptable electronic band structures, strong nonlinear susceptibilities, high LIDTs, and excellent physicochemical stability.[4] While over 500 compounds in this family have been explored to date, research efforts remain heavily concentrated on systems containing d^{10}-configured metal centers, leaving those with alternative electron configurations—such as manganese-based compounds with a d^5 configuration—relatively underexplored. Despite their limited investigation, the known Mn-based IR-NLO materials already exhibit remarkable structural diversity.[5–22] These range from simple chalcogenides (*e.g.*, $RbMn_4In_5Se_{12}$,[5] $Pb_{0.65}Mn_{2.85}Ga_3S_8$,[7] and Li_2MnSnS_4 [10]) to complex heteroanionic systems including oxychalcogenides (*e.g.*, $Ba_{10}In_2Mn_{11}Si_3O_{12}S_{18}$ [12] and $Eu_2MnGe_2OS_6$ [13]) and salt-inclusion chalcogenides (*e.g.*, $[Ba_4Cl_2][MnGa_4Se_{10}]$[16]). However, a critical challenge persists across these systems: their relatively narrow E_g fundamentally limits practical utility by inducing TPA and constraining the LIDT. Consequently, achieving a balanced combination of wide E_g (>3.0 eV) and strong SHG response (>1.0 × $AgGaS_2$) represents a pivotal yet unresolved

[a]*College of Chemistry and Materials Science, Fujian Normal University, Fuzhou 350002, China. E-mail: linhua@fjirsm.ac.cn, qlzhu@fjirsm.ac.cn*
[b]*State Key Laboratory of Structural Chemistry, Fujian Institute of Research on the Structure of Matter, Chinese Academy of Sciences, Fuzhou 350002, China. E-mail: ranmaoyin8@gmail.com*
[c]*Fujian College, University of Chinese Academy of Sciences, Fuzhou 350002, China*
[d]*Yunnan Key Laboratory of Electromagnetic Materials and Devices, School of Materials and Energy, Yunnan University, Kunming 650500, China*
[e]*School of Environmental and Materials Engineering, Yantai University, Yantai 264005, China*

pursuit in the development of high-performance Mn-based IR-NLO materials.

Beyond the performance limitations previously discussed, a more fundamental challenge in the development of Mn-based IR-NLO materials lies in the intentional design of noncentrosymmetric (NCS) structures—a strict prerequisite for any second-order NLO material.[23] Over decades, multiple synthetic strategies have been developed to promote NCS formation, among which chemical substitution has gained considerable attention due to its operational simplicity and structural predictability.[24] This approach typically employs a known centrosymmetric (CS) parent phase as a template, where targeted replacement of cationic or anionic motifs induces symmetry breaking, thereby activating the SHG response. Notable successes of this strategy include the transformation from CS-$CsGaS_2$ to NCS-$[CsBa_2Cl][Ga_4S_8]$,[25] CS-$Rb_4P_2S_6$ to NCS-$RbBiP_2S_6$,[26] CS-$SnBr_2$ to NCS-$Sn_7Br_{10}S_2$,[27] and CS-$PbBr_2$ to NCS-Pb_4SeBr_6.[28] Building on this methodology, our group recently demonstrated that chemical substitution can be strategically applied to wide-E_g CS templates to simultaneously achieve a large SHG response and retain a wide E_g. Representative examples include: CS-$SrGeO_3$ to NCS-$SrGeOSe_2$ (E_g = 3.16 eV, SHG = 1.3 × $AgGaS_2$),[29] CS-Sr_2GaS_4 to NCS-$SrCdSiS_4$ (E_g = 3.61 eV, SHG = 1.1 × $AgGaS_2$),[30] and CS-$Cs_3[Sb_3O_6][Ge_2O_7]$ to NCS-$Nd_3[Ga_3O_3S_3][Ge_2O_7]$ (E_g = 4.35 eV, SHG = 0.8 × $AgGaS_2$).[31] These results highlight the potential of rational substitution strategies to overcome the traditional trade-off between wide E_g and large SHG response—paving a viable pathway toward high-performance Mn-based NLO systems.

Based on the aforementioned design strategy, we herein report the rational synthesis of a novel Mn-based IR-NLO candidate, $Sr_3MnGe_2S_8$, through a partial cation substitution approach, starting from the wide-E_g CS phase Sr_2GeS_4 as a structural template.[32] The resulting $Sr_3MnGe_2S_8$ achieves an outstanding balance of key IR-NLO properties, exhibiting a strong SHG response (2.4 × $AgGaS_2$ at 2050 nm), a high LIDT (13.4 × $AgGaS_2$), and a wide E_g of 3.06 eV. These merits place it

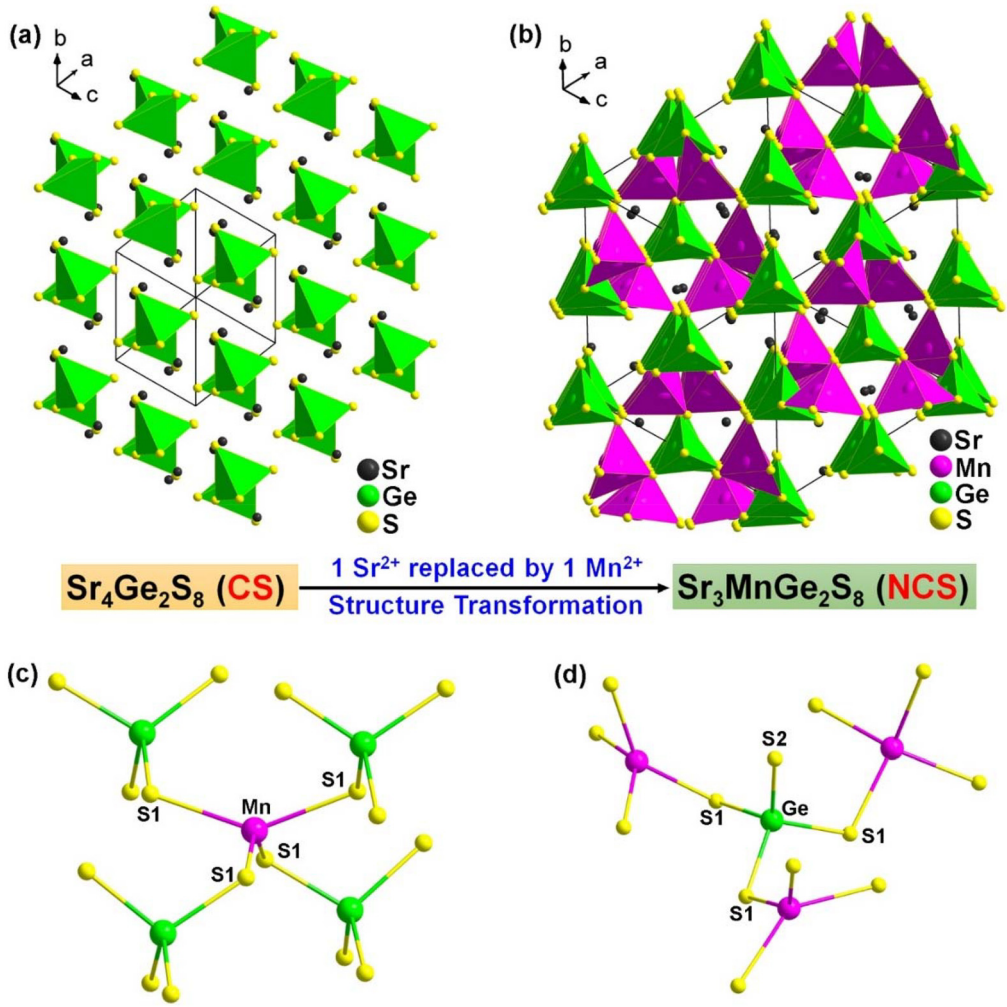

Fig. 1 Structural evolution from (a) CS Sr_2GeS_4 to (b) NCS $Sr_3MnGe_2S_8$ *via* partial cation substitution. The local coordination environments of the (c) $[MnS_4]$ and (d) $[GeS_4]$ tetrahedral units in the resulting $Sr_3MnGe_2S_8$ structure are also displayed.

Table 1 Crystal data and structure refinement for $Sr_3MnGe_2S_8$

Molecular formula	$Sr_3MnGe_2S_8$
CCDC number	2488264
Formula weight	719.46
Crystal system	Cubic
Space group	$I\bar{4}3d$
Temperature (K)	293(2)
Radiation	Mo K_α (λ = 0.71073)
$F(000)$	2648.0
a (Å)	13.97941(15)
α (°)	90
V (Å^3)	2731.91(9)
Z	8
$\rho_{cal.}$ (g cm^{-3})	3.50
μ (mm^{-1})	25.6
GOOF on F^2	1.08
Flack factor	0.04(3)
R_1, wR_2 [$I > 2\sigma(I)$]^a	0.0413, 0.1056
R_1, wR_2 (all data)^a	0.0428, 0.1079
Largest diff. peak and hole (e Å^{-3})	0.82/−1.66

$^a R_1 = \sum||F_o| - |F_c||/\sum|F_o|$, $wR_2 = \{\sum w[(F_o)^2 - (F_c)^2]^2/\sum w[(F_o)^2]^2\}^{1/2}$.

among the top-performing Mn-based chalcogenides reported to date. This work comprehensively describes its synthesis, crystal structure, optical properties, and the underlying structure–property relationships.

Results and discussion

The successful implementation of a chemical substitution strategy for structural transformation and IR-NLO material design critically depends on the judicious selection of a parent structure. In this work, the CS Sr_2GeS_4 was chosen as the template based on two key considerations. First, it contains conventional NLO-active motifs—specifically, isolated [GeS_4] tetrahedra—that are essential for generating a SHG response.[33] Second, its zero-dimensional (0D) structural architecture (Fig. 1a), characterized by well-separated structural units, contributes to a wide experimental E_g (3.46 eV), which is highly

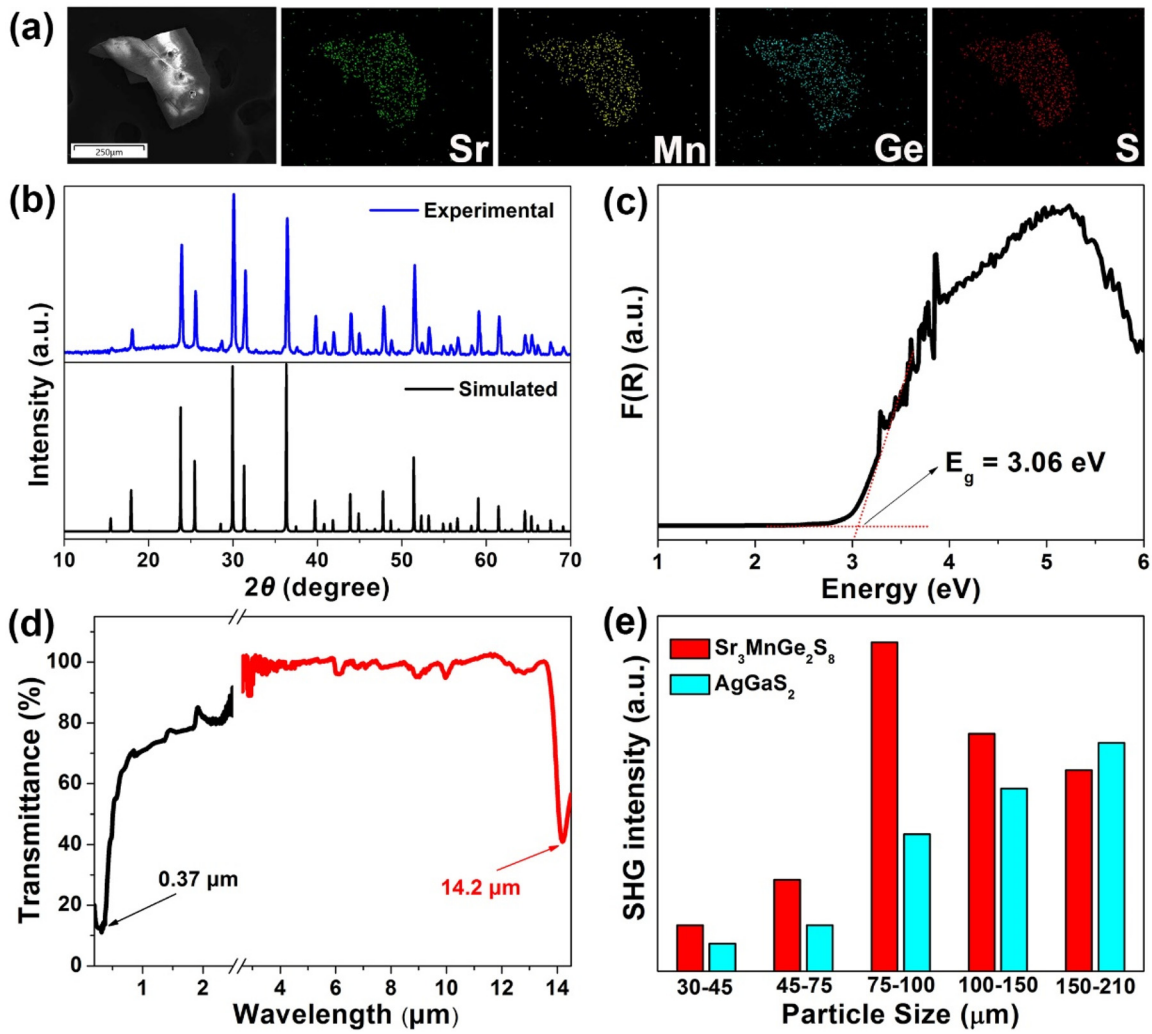

Fig. 2 Characterization of $Sr_3MnGe_2S_8$: (a) SEM image with the corresponding elemental maps, (b) experimental (blue) and simulated (black) powder XRD patterns, (c) solid-state diffuse reflectance spectrum, (d) optical transmission spectra across UV-Vis-NIR and mid-IR regions, and (e) particle size-dependent SHG responses relative to the reference $AgGaS_2$.

desirable for achieving a high LIDT.[34] By partially substituting Sr^{2+} with transition-metal Mn^{2+}, we aimed to leverage the inherent size mismatch to break inversion symmetry—inducing a CS-to-NCS transition—while largely retaining the wide E_g characteristic imparted by the parent structure. Single-crystal X-ray diffraction (XRD) analysis confirms that $Sr_3MnGe_2S_8$ crystallizes in the cubic crystal system with the NCS space group $I\bar{4}3d$ (no. 220). The unit cell parameters are $a = b = c = 13.9794(2)$ Å (Table 1). The asymmetric unit comprises one independent Sr atom (Wyckoff site 24*d*), one Ge atom (16*c*), one Mn atom (12*a*), and two S atoms (sites 48*e* and 16*c*) (Table S1). As depicted in Fig. 1b, the crystal structure of $Sr_3MnGe_2S_8$ is characterized by Mn^{2+} and Ge^{4+} ions in tetrahedral coordination with S atoms, forming $[MnS_4]$ and $[GeS_4]$ units. These tetrahedra interconnect through vertex-sharing, assembling into a three-dimensional (3D) anionic $[MnGe_2S_8]^{6-}$ framework, charge-balanced by Sr^{2+} cations residing in the interstitial sites. Fig. 1c and d illustrate the local coordination geometry of the $[MnS_4]$ and $[GeS_4]$ tetrahedra, respectively. It is noteworthy that each $[MnS_4]$ tetrahedron shares its four S1 atoms with four adjacent $[GeS_4]$ units. In contrast, the $[GeS_4]$ tetrahedron on the three-fold axis is surrounded by three distorted $[MnS_4]$ tetrahedra *via* shared S1 atoms, whereas its S2 atom remains as the terminal atom.

A key structural consequence of the partial substitution of Sr^{2+} by Mn^{2+} is the pronounced distortion observed in both the $[GeS_4]$ and $[MnS_4]$ tetrahedra, attributable to the ionic size mismatch between the substituents. In $Sr_3MnGe_2S_8$, the degree of distortion of the $[GeS_4]$ unit is larger than that in the parent Sr_2GeS_4 structure (15.44° *vs.*14.88°), as quantified by the formula $\sum = \sum_{i=1}^{6} (|\varphi_i - 109.47°|)$.[35] Similarly, the newly formed $[MnS_4]$ tetrahedron displays substantial angular distortion, with a maximum S–Mn–S bond angle of 139.67° and a corresponding gaint degree of distortion of 110.94° (Tables S2 and S3). The local dipole moment also serves as a metric for the tetrahedral distortion, yielding values of 0.84 D and 28.55 D for the $[GeS_4]$ and $[MnS_4]$ units, respectively.[36] Moreover, the charge-balancing Sr atoms exhibit notable differences in their coordination configuration and structure assembly. Specifically, Sr is six-coordinate within the CS Sr_2GeS_4, constituting a 2D layered structure. Conversely, in the NCS $Sr_3MnGe_2S_8$, Sr adopts an eight-coordinate geometry, resulting in a 3D network structure, as shown in Fig. S1. These geometric perturbations collectively underscore the efficacy of chemical substitution in modulating local symmetry and bonding geometry, which is critical for activating and enhancing second-order SHG responses.

The pale yellow crystalline compound $Sr_3MnGe_2S_8$ was synthesized *via* a high-temperature solid-state reaction under vacuum, using stoichiometric mixtures of Sr, Mn, Ge, and S. The resulting product (with a yield of approximately 70%) demonstrated excellent stability, remaining unaltered after more than one year of storage in ambient air (see the SI for details). Energy dispersive X-ray spectroscopy (EDX) confirmed the homogeneous distribution of Sr, Mn, Ge, and S throughout the crystal, with an average atomic ratio of approximately 3 : 1.1 : 2 : 7.9 (Fig. 2a and Fig. S2), in good agreement with the stoichiometry derived from single-crystal XRD structure analysis. Phase purity was further verified by powder XRD, as shown in Fig. 2b. UV-vis-NIR absorption spectroscopy revealed that $Sr_3MnGe_2S_8$ possesses a wide optical E_g of 3.06 eV, as estimated using the Kubelka–Munk function[37] (Fig. 2c). This

Table 2 Properties comparison of the reported Mn-based IR-NLO chalcogenides

Number	Compounds	Unit cell	Space group	E_g (eV)	SHG (×$AgGaS_2$)	Ref.
1	$CsMn_4In_5Te_{12}$	*R*3 (no. 146)	Trigonal	1.48	0.3	5
2	$K_3Mn_2Sb_3S_8$	$I\bar{4}2m$ (no. 121)	Tetragonal	1.58	0.4	6
3	$Rb_3Mn_2Sb_3S_8$	$I\bar{4}2m$ (no. 121)	Tetragonal	1.61	0.3	6
4	$Pb_{0.72}Mn_{2.84}Ga_{2.95}Se_8$	$P\bar{6}$ (no. 174)	Hexagonal	1.65	4.4	7
5	$RbMn_4In_5Se_{12}$	*R*3 (no. 146)	Trigonal	1.76	4.4	5
6	$CsMn_4In_5Se_{12}$	*R*3 (no. 146)	Trigonal	1.79	4.0	5
7	$BaMnSnS_4$	*Fdd*2 (no. 43)	Orthorhombic	1.90	1.2	8
8	$CsMnAs_3S_6$	$I\bar{4}$ (no. 82)	Trigonal	2.02	0.9	9
9	Li_2MnSnS_4	$Pmn2_1$ (no. 33)	Orthorhombic	2.03	0.5	10
10	$RbMnAs_3S_6$	*R*3 (no. 146)	Trigonal	2.16	1.1	9
11	$Pb_{0.65}Mn_{2.85}Ga_3S_8$	$P\bar{6}$ (no. 174)	Hexagonal	2.25	1.5	7
12	$Sr_3MnSn_2S_8$	$I\bar{4}3d$ (no. 220)	Cubic	2.33	1.0	11
13	$Ba_{10}In_2Mn_{11}Si_3O_{12}S_{18}$	$I\bar{4}3m$ (no. 217)	Cubic	2.38	3 × α-SiO_2	12
14	$Eu_2MnGe_2OS_6$	$P\bar{4}2_1m$ (no. 113)	Tetragonal	2.40	0.3	13
15	$Ba_6Cu_{2.2}Mn_{0.8}(SnS_4)_4$	$I\bar{4}3d$ (no. 220)	Cubic	2.5	2.4	14
16	$Ba_6(Cu_2Mn)Ge_4S_{16}$	$I\bar{4}3d$ (no. 220)	Cubic	2.70	2.2	15
17	$[Ba_4Cl_2][MnGa_4Se_{10}]$	$I\bar{4}$ (no. 82)	Tetragonal	2.78	1.0	16
18	$[K_4Cl][MnGa_9S_{16}]$	*P*1 (no. 1)	Triclinic	3.02	0.6	17
19	Li_2MnGeS_4	$Pmn2_1$ (no. 33)	Orthorhombic	3.07	0.5	18
20	$[K_3Cl][Mn_2Ga_6S_{12}]$	*P*31c (no. 159)	Trigonal	3.17	3.10	19
21	$CsMn_3Ga_5S_{11}$	*Pc* (no. 7)	Monoclinic	3.23	0.8	20
22	$RbMn_3Ga_5S_{11}$	*Pc* (no. 7)	Monoclinic	3.27	0.7	20
23	$K_3Rb_3[K_3Cl][Li_2Mn_4Ga_{12}S_{27}]$	$P6_3mc$ (no. 186)	Hexagonal	3.31	1.1	21
24	$Sr_2MnGe_2OS_6$	$P\bar{4}2_1m$ (no.113)	Tetragonal	3.51	0.3	22
★	**$Sr_3MnGe_2S_8$**	***I*$\bar{4}$3*d* (no. 220)**	**Cubic**	**3.06**	**2.4**	**This work**

value represents one of the largest E_g reported to date among Mn-based IR-NLO materials, exceeding the threshold of 3.0 eV (see Table 2 for details). Notably, the optical E_g of $Sr_3MnGe_2S_8$ is substantially broader than those of well-established IR-NLO crystals such as $AgGaS_2$ (2.56 eV),[38] $AgGaSe_2$ (1.83 eV),[39] and $ZnGeP_2$ (2.0 eV).[2] A large E_g is beneficial for minimizing TPA and achieving a high LIDT. In light of this, we evaluated $Sr_3MnGe_2S_8$'s performance in high-power applications by measuring its powder LIDT. The obtained value of 37.52 MW cm^{-2} at 1064 nm is 13.4 times that of $AgGaS_2$ (2.8 MW cm^{-2}).[40] Additionally, transmission measurements based on the single-crystal sample indicate that $Sr_3MnGe_2S_8$ exhibits a broad transparency window spanning from 0.37 μm (UV-Vis) to 14.2 μm (far-IR) (Fig. 2d). This value is comparable to recently reported IR-NLO materials, such as $Cs_3In(In_4Se_7)(P_2Se_6)$ (0.41–19.5 μm), $[Ba_{22}(SO_4)_5][Zn_{14}Ga_{18}S_{58}]$ (0.35–10.2 μm), $[K_4BaCl_2][In_6Se_{11}]$ (0.7–17.1 μm), and $[Ba_4Cl_2][CdGa_4S_{10}]$ (0.28–18.6 μm).[41] The compound also displays remarkable thermal stability, maintaining its structural integrity up to 1100 K under a nitrogen atmosphere, as evidenced by thermogravimetric analysis (Fig. S3). The exceptional thermal stability of this compound—outperforming recent chalcogenides such as $LiPb_3GeS_4Cl_3$ (693 K), β-$EuZnGeS_4$ (1073 K), and $(Na_3Rb)Hg_2Ge_2S_8$ (717 K)[42]—makes it highly promising for applications demanding harsh-environment operation. Owing to its NCS crystal structure, the NLO properties of $Sr_3MnGe_2S_8$ were systematically evaluated using the powder SHG method. Polycrystalline samples of $Sr_3MnGe_2S_8$, along with $AgGaS_2$ as a reference, were carefully ground and sieved into five distinct particle size ranges. SHG measurements were conducted using a 2050 nm laser. As shown in Fig. 2e, the SHG intensity of $Sr_3MnGe_2S_8$ does not increase monotonically with the increase of particle size, indicating non-phase-matching behavior—consistent with its cubic crystal system, which lacks sufficient bire-

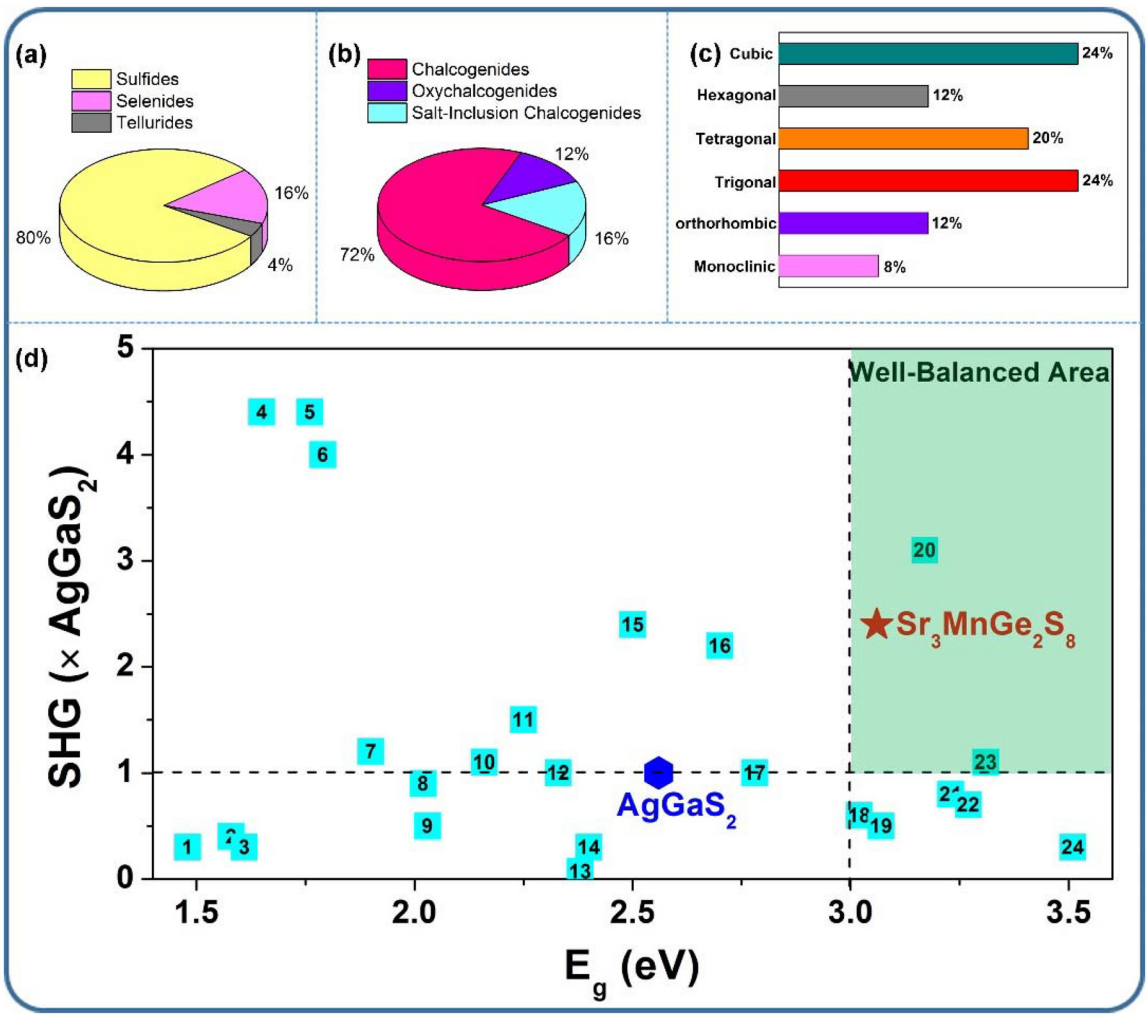

Fig. 3 Statistical distribution of Mn-based IR-NLO chalcogenides categorized by (a and b) chemical composition and (c) crystallographic system. (d) Mapping the balance between SHG and E_g for Mn-based IR-NLO chalcogenides. The outlined area identifies the most promising candidates with a wide E_g (>3.0 eV) and large SHG efficiency (>1.0 × $AgGaS_2$). Detailed data are provided in Table S2.

fringence for phase matching. Notably, $Sr_3MnGe_2S_8$ exhibits a strong SHG response, reaching approximately 2.4 times that of $AgGaS_2$ in the particle size range of 75–100 μm (Fig. 2e).

To contextualize the performance of the newly discovered $Sr_3MnGe_2S_8$, we have benchmarked it against known Mn-based IR-NLO materials. As shown in Fig. 3 and summarized in Table 2, sulfides represent the majority of materials in this category, comprising 80% of reported compounds, whereas selenides and tellurides account for 16% and 4%, respectively (Fig. 3a). When classified by anionic composition, these chalcogenides can be categorized into two groups: single-anion chalcogenides, which constitute the predominant fraction (72%), and mixed-anion chalcogenides, representing a smaller proportion (28%). The latter includes oxychalcogenides (12%) and salt-inclusion chalcogenides (16%) (Fig. 3b). Statistical analysis indicates that Mn-based IR-NLO chalcogenides crystallize in all six crystal systems, with the following distribution: cubic (24%), tetragonal (20%), orthorhombic (12%), trigonal (24%), hexagonal (12%), and monoclinic (8%) (Fig. 3c). This distribution reflects a pronounced preference for high-symmetry systems (approximately 80%), whereas low-symmetry structures, such as the triclinic and monoclinic system, are relatively uncommon. Fig. 3d summarizes two critical performance indicators for these compounds—the SHG response and the E_g—with detailed data provided in Table 2. Notably, $Sr_3MnGe_2S_8$ achieves a remarkable balance between a wide E_g (>3.0 eV) and a strong SHG response (>1.0 × $AgGaS_2$), a combination that effectively overcomes the typical performance trade-off in Mn-based NLO systems.

To elucidate the optical properties and structure–performance correlations of the title compound, first-principles calculations of DFT were conducted using the VASP package. The electronic band structure along high-symmetry paths (Fig. S4) confirms that $Sr_3MnGe_2S_8$ is an indirect bandgap semiconductor with a theoretical E_g of 2.23 eV. The computed value is moderately lower than the experimental result, a discrepancy commonly associated with the discontinuity in the exchange–correlation energy inherent to the GGA.[43] The partial density of states (PDOS) in Fig. 4 reveals pronounced orbital hybridization between Mn and S, as well as between Ge and S, across both the valence bands (VBs) and conduction bands (CBs), indicative of strong covalent character. The upper VB is mainly constituted by Ge 4s, Ge 4p, Mn 3d, and S 3p orbitals, while the lower CB is primarily contributed by Ge 4s, Ge 4p, Mn 3d, and S 3p orbitals. Since electronic transitions near the band edges are critical in governing optical behavior, the Ge–S and Mn–S groups are considered key structural units responsible for the optical E_g and NLO properties of $Sr_3MnGe_2S_8$. Furthermore, the SHG coefficients of $Sr_3MnGe_2S_8$ were evaluated based on the electronic structure using the length-gauge formalism.[44] In accordance with Kleinman's symmetry[45] and the $I\bar{4}3d$ space group, only one independent SHG tensor element, d_{14}, is present, and its value is calculated as 15.72 pm V^{-1}, showing good consistency with experimental findings.

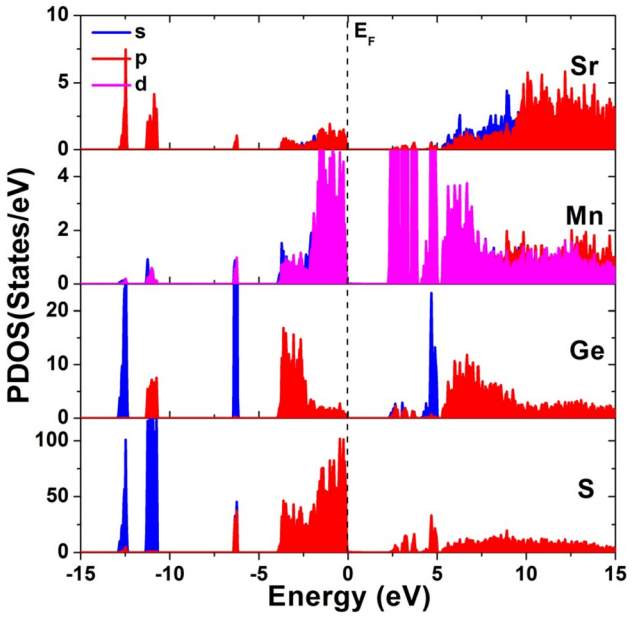

Fig. 4 The partial density of states (PDOS) of $Sr_3MnGe_2S_8$.

Conclusions

In summary, a novel NCS Mn-based quaternary sulfide, $Sr_3MnGe_2S_8$, has been successfully synthesized *via* an equivalent partial cation substitution strategy, using the CS compound Sr_2GeS_4 as the parent template. This material demonstrates outstanding IR-NLO performance, characterized by a strong SHG response (2.4 × $AgGaS_2$ at 2050 nm), a wide E_g (3.06 eV), a high LIDT (13.4 × $AgGaS_2$), and a broad transparency range (0.37–14.2 μm). These properties are attributed to the synergistic effect arising from the distortion and favorable alignment of the constituent $[MnS_4]$ and $[GeS_4]$ tetrahedral units. Notably, $Sr_3MnGe_2S_8$ stands out as one of the very few Mn-based chalcogenides that simultaneously surpass the benchmark thresholds of large SHG efficiency (>1.0 × $AgGaS_2$) and wide E_g (>3.0 eV). Through detailed structural and theoretical analysis, we establish that the partial substitution of Sr by Mn not only triggers a CS-to-NCS structural transformation but also significantly enhances the NLO activity. This work provides an effective chemical design strategy for achieving balanced NLO performance and opens a viable pathway for the discovery of high-performance IR-NLO materials through targeted structural engineering.

Author contributions

A-Lan Xu: investigation, formal analysis, writing – original draft. Mao-Yin Ran: investigation, formal analysis, writing – review & editing. Zuju Ma: methodology, validation. Xin-Tao Wu: conceptualization, writing – review & editing. Hua Lin: supervision, conceptualization, writing – review & editing. Qi-Long Zhu: supervision, writing – review & editing.

Conflicts of interest

There are no conflicts to declare.

Data availability

The data supporting this article have been included as part of the supplementary information (SI). Supplementary information: additional experimental and theoretical results, together with additional tables and figures. See DOI: https://doi.org/10.1039/d5qi02182k.

CCDC 2488264 contains the supplementary crystallographic data for this paper.[46]

Acknowledgements

This work was supported by the National Natural Science Foundation of China (22175175), Natural Science Foundation of Fujian Province (2022L3092 and 2023H0041). The authors thank Prof. Bing-Xuan Li at FJIRSM for helping with the NLO measurements, Prof. Long-Hua Li at Jiangsu University and Prof. Yong-Fan Zhang at Fuzhou University for helping with the DFT calculations.

References

1 (*a*) T. Schneider, *Nonlinear optics in telecommunications*, Springer Science & Business Media, 2004; (*b*) M. G. Papadopoulos, A. J. Sadlej and J. Leszczynski, *Non-linear optical properties of matter*, Springer, 2006; (*c*) A. Newell, *Nonlinear Optics*, CRC Press, 2018; (*d*) H. D. Yang, M. Y. Ran, W. B. Wei, X. T. Wu, H. Lin and Q. L. Zhu, Recent advances in IR nonlinear optical chalcogenides with well-balanced comprehensive performance, *Mater. Today Phys.*, 2023, **35**, 101127; (*e*) J. X. Zhang, P. Feng, M. Y. Ran, X. T. Wu, H. Lin and Q. L. Zhu, Ga-based IR nonlinear optical materials: synthesis, structures, and properties, *Coord. Chem. Rev.*, 2024, **502**, 215617.

2 (*a*) G. D. Boyd, H. Kasper and J. H. McFee, Linear and nonlinear optical properties of $AgGaS_2$, $CuGaS_2$, and $CuInS_2$, and theory of the wedge technique for the measurement of nonlinear coefficients, *IEEE J. Quantum Electron.*, 1971, **7**, 563–573; (*b*) B. Tell and H. M. Kasper, Optical and Electrical Properties of $AgGaS_2$ and $AgGaSe_2$, *Phys. Rev. B*, 1971, **4**, 4455–4459; (*c*) G. D. Boyd, E. Buehler and F. G. Storz, Linear and Nonlinear Optical Properties of $ZnGeP_2$ and CdSe, *Appl. Phys. Lett.*, 1971, **18**, 301–304.

3 (*a*) K. Wu and S. L. Pan, A review on structure-performance relationship toward the optimal design of infrared nonlinear optical materials with balanced performances, *Coord. Chem. Rev.*, 2018, **377**, 191–208; (*b*) H.-D. Yang, M.-Y. Ran, W.-B. Wei, X.-T. Wu, H. Lin and Q.-L. Zhu, The Rise of Infrared Nonlinear Optical Pnictides: Advances and Outlooks, *Chem. – Asian J.*, 2021, **16**, 3299–3310; (*c*) H. Chen, M.-Y. Ran, W.-B. Wei, X.-T. Wu, H. Lin and Q.-L. Zhu, A comprehensive review on metal chalcogenides with three-dimensional frameworks for infrared nonlinear optical applications, *Coord. Chem. Rev.*, 2022, **470**, 214706; (*d*) S.-P. Guo, Y. Chi and G.-C. Guo, Recent achievements on middle and far-infrared second-order nonlinear optical materials, *Coord. Chem. Rev.*, 2017, **335**, 44–57; (*e*) J.-X. Zhang, M.-Y. Ran, X.-T. Wu, H. Lin and Q.-L. Zhu, An overview of Mg-based IR nonlinear optical materials, *Inorg. Chem. Front.*, 2023, **10**, 5244–5257; (*f*) P. Feng, J.-X. Zhang, M.-Y. Ran, X.-T. Wu, H. Lin and Q.-L. Zhu, Rare-earth-based chalcogenides and their derivatives: an encouraging IR nonlinear optical material candidate, *Chem. Sci.*, 2024, **15**, 5869–5896; (*g*) L. Dong, S. Zhang, P. Gong, L. Kang and Z. Lin, Evaluation and prospect of Mid-Infrared nonlinear optical materials in f^0 rare earth (RE = Sc, Y, La) chalcogenides, *Coord. Chem. Rev.*, 2024, **509**, 215805.

4 (*a*) H. Chen, W. B. Wei, H. Lin and X. T. Wu, Transition-metal-based chalcogenides: A rich source of infrared nonlinear optical materials, *Coord. Chem. Rev.*, 2021, **448**, 214154; (*b*) W. F. Zhou, J. J. Wu, W. L. Liu and S. P. Guo, Ag-based chalcogenides and derivatives as promising infrared nonlinear optical materials, *Coord. Chem. Rev.*, 2023, **477**, 214950; (*c*) B. Zhang, S.-H. Zhou, B.-X. Li, X.-T. Wu, H. Lin and Q.-L. Zhu, Exploring new horizons in mid-to-far infrared nonlinear optical crystals: the significant potential of trigonal pyramidal $[TeS_3]^{2-}$ functional units, *Chem. Sci.*, 2025, **16**, 3218–3227.

5 H. Lin, L. Chen, L. J. Zhou and L. M. Wu, Functionalization Based on the Substitutional Flexibility: Strong Middle IR Nonlinear Optical Selenides $AX^{II}{}_4X^{III}{}_5Se_{12}$, *J. Am. Chem. Soc.*, 2013, **135**, 12914–12921.

6 Y. Xiao, M. M. Chen, Y. Y. Shen, P. F. Liu, H. Lin and Y. Liu, $A_3Mn_2Sb_3S_8$ (A = K and Rb): a new type of multifunctional infrared nonlinear optical material based on unique three-dimensional open frameworks, *Inorg. Chem. Front.*, 2021, **8**, 2835–2843.

7 M. L. Zhou, X. X. Jiang, Y. W. Guo, Z. S. Lin, J. Y. Yao and Y. C. Wu, $Pb_{0.65}Mn_{2.85}Ga_3S_8$ and $Pb_{0.72}Mn_{2.84}Ga_{2.95}Se_8$: Two Quaternary Metal Chalcognides with Open-Tunnel-Framework Structures Displaying Intense Second Harmonic Generation Responses and Interesting Magnetic Properties, *Inorg. Chem.*, 2017, **56**, 8454–8461.

8 Y. J. Lin, R. Ye, L. Q. Yang, X. M. Jiang, B. W. Liu, H. Y. Zeng and G. C. Guo, $BaMnSnS_4$ and $BaCdGeS_4$: infrared nonlinear optical sulfides containing highly distorted motifs with centers of moderate electronegativity, *Inorg. Chem. Front.*, 2019, **6**, 2365.

9 R. Ye, B. W. Liu, X. M. Jiang, J. Lu, H. Y. Zeng and G. C. Guo, $AMnAs_3S_6$ (A = Cs, Rb): Phase-Matchable Infrared Nonlinear Optical Functional Motif $[As_3S_6]^{3-}$ Obtained via Surfactant–Thermal Method, *ACS Appl. Mater. Interfaces*, 2020, **12**, 53950–53956.

10 K. P. Devlin, A. J. Glaid, J. A. Brant, J. H. Zhang, M. N. Srnec, D. J. Clark, Y. S. Kim, J. I. Jang, K. R. Daley,

M. A. Moreau, J. D. Madura and J. A. Aitken, Polymorphism and second harmonic generation in a novel diamond-like semiconductor: Li_2MnSnS_4, *J. Solid State Chem.*, 2015, **231**, 256–266.

11 C. Liu, D. J. Mei, W. Z. Cao, Y. Yang, Y. D. Wu, G. B. Li and Z. S. Lin, Mn-Based tin sulfide $Sr_3MnSn_2S_8$ with a wide band gap and strong nonlinear optical response, *J. Mater. Chem. C*, 2019, **7**, 1146–1150.

12 A. Y. Wang, M. Y. Ran, X. T. Wu, H. Lin and Q. L. Zhu, $Ba_{10}In_2Mn_{11}Si_3O_{12}S_{18}$: First Hexanary Oxychalcogenide Containing an Infrequent Three-Dimensional Noncentrosysmmetric Framework, *Inorg. Chem.*, 2024, **63**, 4022–4027.

13 N. Zhang, X. Huang, W. D. Yao, Y. Chen, Z. R. Pan, B. X. Li, W. L. Liu and S. P. Guo, $Eu_2MGe_2OS_6$ (M = Mn, Fe, Co): Three Melilite-Type Rare-Earth Oxythiogermanates Exhibiting Balanced Nonlinear-Optical Behaviors, *Inorg. Chem.*, 2023, **62**, 16299–16303.

14 B. H. Ji, K. Wu, Y. H. Chen, F. Wang, A. J. Rossini, B. B. Zhang and J. Wang, $Ba_6(Cu_xZ_y)Sn_4S_{16}$ (Z = Mg, Mn, Zn, Cd, In, Bi, Sn): High Chemical Flexibility Resulting in Good Nonlinear-Optical Properties, *Inorg. Chem.*, 2022, **61**, 2640–2651.

15 G. Cicirello, K. Wu and J. Wang, Synthesis, crystal structure, linear and nonlinear optical properties of quaternary sulfides $Ba_6(Cu_2X)Ge_4S_{16}$ (X=Mg, Mn, Cd), *J. Solid State Chem.*, 2021, **300**, 122226.

16 Y. Y. Li, P. F. Liu, L. Hu, L. Chen, H. Lin, L. J. Zhou and L. M. Wu, Strong IR NLO Material $Ba_4MGa_4Se_{10}Cl_2$: Highly Improved Laser Damage Threshold via Dual Ion Substitution Synergy, *Adv. Opt. Mater.*, 2015, **3**, 957–966.

17 S. M. Pei, M. S. Zhang, F. Wu, Y. Guo, X. M. Jiang, B. W. Liu and G. C. Guo, Salt-inclusion chalcogenides with d-orbital components: unveiling remarkable nonlinear optical properties and dual-band photoluminescence, *Chem. Sci.*, 2024, **15**, 13753–13759.

18 J. A. Brant, D. J. Clark, Y. S. Kim, J. I. Jang, A. Weiland and J. A. Aitken, Outstanding Laser Damage Threshold in Li_2MnGeS_4 and Tunable Optical Nonlinearity in Diamond-Like Semiconductors, *Inorg. Chem.*, 2015, **54**, 2809.

19 B. W. Liu, S. M. Pei, X. M. Jiang and G. C. Guo, Broad transparency and wide band gap achieved in a magnetic infrared nonlinear optical chalcogenide by suppressing d–d transitions, *Mater. Horiz.*, 2022, **9**, 1513–1517.

20 M. M. Chen, S. H. Zhou, W. B. Wei, X. T. Wu, H. Lin and Q. L. Zhu, Phase Matchability Transformation in the Infrared Nonlinear Optical Materials with Diamond-Like Frameworks, *Adv. Opt. Mater.*, 2022, **10**, 2102123.

21 S. M. Pei, B. W. Liu, W. F. Chen, X. M. Jiang and G. C. Guo, Breaking the bottleneck of simultaneously wide band gap and large nonlinear optical coefficient by a "pore reconstruction" strategy in a salt-inclusion chalcogenide, *Mater. Horiz.*, 2023, **10**, 2921–2926.

22 M. Y. Ran, S. H. Zhou, B. X. Li, W. B. Wei, X. T. Wu, H. Lin and Q. L. Zhu, Enhanced Second-Harmonic-Generation Efficiency and Birefringence in Melillite Oxychalcogenides $Sr_2MGe_2OS_6$ (M = Mn, Zn, and Cd), *Chem. Mater.*, 2022, **34**, 3853–3861.

23 (*a*) K. M. Ok, Toward the Rational Design of Novel Noncentrosymmetric Materials: Factors Influencing the Framework Structures, *Acc. Chem. Res.*, 2016, **49**, 2774; (*b*) X. Liu, Y. C. Yang, M. Y. Li, L. Chen and L. M. Wu, Anisotropic structure building unit involving diverse chemical bonds: a new opportunity for high-performance second-order NLO materials, *Chem. Soc. Rev.*, 2023, **52**, 8699.

24 (*a*) H. Lin, W. B. Wei, H. Chen, X. T. Wu and Q. L. Zhu, Rational design of infrared nonlinear optical chalcogenides by chemical substitution, *Coord. Chem. Rev.*, 2020, **406**, 213150; (*b*) M.-Y. Ran, A.-Y. Wang, W.-B. Wei, X.-T. Wu, H. Lin and Q.-L. Zhu, Recent progress in the design of IR nonlinear optical materials by partial chemical substitution: structural evolution and performance optimization, *Coord. Chem. Rev.*, 2023, **481**, 215059; (*c*) W. Zhou and S. P. Guo, Rational Design of Novel Promising Infrared Nonlinear Optical Materials: Structural Chemistry and Balanced Performances, *Acc. Chem. Res.*, 2024, **57**, 648.

25 B. W. Liu, X. M. Jiang, H. Y. Zeng and G.-C. Guo, $[ABa_2Cl][Ga_4S_8]$ (A = Rb, Cs): Wide-Spectrum Nonlinear Optical Materials Obtained by Polycation-Substitution-Induced NLO-Functional Motif Ordering, *J. Am. Chem. Soc.*, 2020, **142**, 10641–10645.

26 M. M. Chen, S. H. Zhou, W. B. Wei, B. X. Li, M.-Y. Ran, X. T. Wu, H. Lin and Q. L. Zhu, $RbBiP_2S_6$: A Promising IR Nonlinear Optical Material with a Giant Second-Harmonic Generation Response Designed by Aliovalent Substitution, *ACS Mater. Lett.*, 2022, **4**, 1264–1269.

27 X. H. Li, Z. H. Shi, M. Yang, W. Liu and S. P. Guo, $Sn_7Br_{10}S_2$: The First Ternary Halogen-Rich Chalcohalide Exhibiting a Chiral Structure and Pronounced Nonlinear Optical Properties, *Angew. Chem., Int. Ed.*, 2022, **61**, e202115871.

28 J. Wang, H. Wu, H. Yu, Z. Hu, J. Wang and Y. Wu, Pb_4SeBr_6: A Congruently Melting Mid-Infrared Nonlinear Optical Material with Excellent Comprehensive Performance, *Adv. Opt. Mater.*, 2022, **10**, 2102673.

29 M. Y. Ran, Z. Ma, H. Chen, B. Li, X. T. Wu, H. Lin and Q.-L. Zhu, Partial Isovalent Anion Substitution to Access Remarkable Second-Harmonic Generation Response: A Generic and Effective Strategy for Design of Infrared Nonlinear Optical Materials, *Chem. Mater.*, 2020, **32**, 5890–5896.

30 H. D. Yang, M. Y. Ran, S. H. Zhou, X. T. Wu, H. Lin and Q. L. Zhu, Rational Design via Dual-Site Aliovalent Substitution Leads to an Outstanding IR Nonlinear Optical Material with Well-Balanced Comprehensive Properties, *Chem. Sci.*, 2022, **13**, 10725.

31 M. Y. Ran, S. H. Zhou, W. B. Wei, B. X. Li, X. T. Wu, H. Lin and Q. L. Zhu, Rational Design of a Rare-Earth Oxychalcogenide $Nd_3[Ga_3O_3S_3][Ge_2O_7]$ with Superior Infrared Nonlinear Optical Performance, *Small*, 2023, **19**, 2300248.

32 M. Jawad, A. U. Rahman, Q. Rafique, S. Azam and F. Ijaz, First principle investigation of structural, electronic, optical and thermoelectric properties of Chalcogenide Sr_2GeX_4 (X = S, Se), *Mater. Sci. Semicond. Process.*, 2024, **173**, 108105.

33 (*a*) G. Li, K. Wu, Q. Liu, Z. Yang and S. Pan, $Na_2ZnGe_2S_6$: A New Infrared Nonlinear Optical Material with Good Balance between Large Second-Harmonic Generation Response and High Laser Damage Threshold, *J. Am. Chem. Soc.*, 2016, **138**, 7422–7428; (*b*) M.-Y. Li, B.-X. Li, H. Lin, Y.-F. Shi, Z. Ma, L.-M. Wu, X.-T. Wu and Q.-L. Zhu, Ternary Mixed-Metal Cd_4GeS_6: Remarkable Nonlinear Optical Properties Based on a Tetrahedral-Stacking Framework, *Inorg. Chem.*, 2018, **57**, 8730–8734; (*c*) K. Wu, Y. Chu, Z. Yang and S. Pan, $A_2SrMIVS_4$ (A = Li, Na; MIV = Ge, Sn) concurrently exhibiting wide bandgaps and good nonlinear optical responses as new potential infrared nonlinear optical materials, *Chem. Sci.*, 2019, **10**, 3963–3968; (*d*) H. Chen, M.-Y. Ran, S.-H. Zhou, X.-T. Wu and H. Lin, Ag_2GeS_3: A Diamond-Like Chalcogenide as an IR Nonlinear Optical Material with Outstanding Second-Harmonic Generation Response, *Adv. Opt. Mater.*, 2024, **12**, 2401100.

34 (*a*) H. Chen, M.-Y. Ran, S.-H. Zhou, X.-T. Wu, H. Lin and Q.-L. Zhu, Simple yet extraordinary: super-polyhedra-built 3D chalcogenide framework of $Cs_5Ga_9S_{16}$ with excellent infrared nonlinear optical performance, *Chin. Chem. Lett.*, 2023, **34**, 107838; (*b*) C.-Y. Zhao, C.-L. Hu, N.-T. Suen, X.-H. Li, H.-P. Xu, W. F. Zhou and S.-P. Guo, Rare-earth substitution induced symmetry breaking for the first Sc-based nonlinear optical chalcogenide with high-performance, *Adv. Sci.*, 2025, **12**, 2411960; (*c*) A.-Y. Wang, S.-H. Zhou, M.-Y. Ran, X.-T. Wu, H. Lin and Q.-L. Zhu, Regulating the Key Performance Parameters for Hg-based IR NLO Chalcogenides via Bandgap Engineering Strategy, *Chin. Chem. Lett.*, 2024, **35**, 109377.

35 Y. X. Zhang, B. X. Li, H. Lin, Z. J. Ma, X. T. Wu and Q. L. Zhu, Impressive second harmonic generation response in a novel phase-matchable NLO-active MOF derived from achiral precursors, *J. Mater. Chem. C*, 2019, **7**, 6217–6221.

36 (*a*) H. K. Izumi, J. E. Kirsch, C. L. Stern and K. R. Poeppelmeier, Examining the out-of-center distortion in the $[NbOF_5]^{2-}$ anion, *Inorg. Chem.*, 2005, **44**, 884–895; (*b*) P. A. Maggard, T. S. Nault, C. L. Stern and K. R. Poeppelmeier, Alignment of acentric $MoO_3F_3{}^{3-}$ anions in a polar material:$(Ag_3MoO_3F_3(Ag_3MoO_4)Cl$, *J. Solid State Chem.*, 2003, **175**, 27–33.

37 P. Kubelka and F. Munk, Ein beitrag zur optik der farbanstriche, *Z. Tech. Phys.*, 1931, **12**, 593–601.

38 (*a*) H. Lin, L. J. Zhou and L. Chen, Sulfides with Strong Nonlinear Optical Activity and Thermochromism: $ACd_4Ga_5S_{12}$ (A = K, Rb, Cs), *Chem. Mater.*, 2012, **24**, 3406–3414; (*b*) H. Chen, Y.-Y. Li, B.-X. Li, P.-F. Liu, H. Lin, Q.-L. Zhu and X.-T. Wu, Salt-Inclusion Chalcogenide $[Ba_4Cl_2][ZnGa_4S_{10}]$: Rational Design of an IR Nonlinear Optical Material with Superior Comprehensive Performance Derived from $AgGaS_2$, *Chem. Mater.*, 2020, **32**, 8012–8019.

39 G. C. Catella, L. R. Shiozawa, J. R. Hietanen, R. C. Eckardt, R. K. Route, R. S. Feigelson, D. G. Cooper and C. L. Marquardt, MidIR absorption in $AgGaSe_2$ optical parametric oscillator crystals, *Appl. Opt.*, 1993, **32**, 3948–3951.

40 (*a*) M.-Y. Ran, S.-H. Zhou, B.-X. Li, X.-T. Wu, H. Lin and Q.-L. Zhu, Balanced IR Nonlinear Optical Performance Achieved by Cation-Anion Module Cosubstitution in V-Based Salt-Inclusion Oxychalcogenides, *Chem. Mater.*, 2024, **36**, 11996; (*b*) P. Feng, S.-H. Zhou, B.-X. Li, J.-X. Zhang, M.-Y. Ran, X.-T. Wu, H. Lin and Q.-L. Zhu, Realizing Excellent Infrared Nonlinear Optical Performance in Eu-based Chalcogenides via Rational Cross Substitution Strategy, *ACS Appl. Mater. Interfaces*, 2024, **16**, 52682–52691.

41 (*a*) Z. Qian, H. Wu, Z. Hu, J. Wang, Y. Wu and H. Yu, $Cs_3In(In_4Se_7)(P_2Se_6)$: A Multi-Chromophore Chalcogenide with Excellent Nonlinear Optical Property Designed by Group Grafting, *Angew. Chem., Int. Ed.*, 2024, **63**, e202400892; (*b*) J.-X. Zhang, M.-Y. Ran, A.-Y. Wang, Z. Ma, X.-T. Wu, H. Lin and Q.-L. Zhu, Discovering Pseudo-Supertetrahedral Functional units in Salt-Inclusion Nonlinear Optical Material $[Ba_{22}(SO_4)_5][Zn_{14}Ga_{18}S_{58}]$, *ACS Mater. Lett.*, 2025, **7**, 1512–1519; (*c*) S.-M. Pei, X.-M. Jiang, B.-W. Liu and G.-C. Guo, Expanding the Spectral Range in T2-Supertetrahedral Nonlinear Optical Chalcogenides via Incorporating Inorganic Polycations, *Angew. Chem., Int. Ed.*, 2025, **64**, e202505421; (*d*) J.-X. Zhang, S.-H. Zhou, X.-T. Wu, H. Lin and Q.-L. Zhu, Nonbonding Electron Inversion-Driven Structural Engineering: Synergistic Enhancement of Linear and Nonlinear Optical Properties, *Angew. Chem., Int. Ed.*, 2025, **64**, e202506658.

42 (*a*) Y. H. Hu, R. X. Wang, S. Zhao, Y. Z. Yang, J. Y. Guo, L. M. Wu and L. Chen, $LiPb_3GeS_4Cl_3$: Quasi-T2-Supertetrahedral 3D Framework Enabling Superior Optical Performance, *Angew. Chem., Int. Ed.*, 2025, e202520065; (*b*) P. Feng, S. H. Zhou, M. Y. Ran, B. X. Li, X. T. Wu, H. Lin and Q. L. Zhu, Isovalent cation substitution drives structural transformation and infrared nonlinear optical activity in Eu-based chalcogenides, *Inorg. Chem. Front.*, 2025, **7**, 2648–2660; (*c*) C. L. Tang, W. H. Xing, F. Liang, M. R. Sun, J. Tang, Z. S. Lin, J. Y. Yao, K. X. Chen, J. Y. Wu, W. L. Yin and B. Kang, Structural modification from centrosymmetric $Rb_4Hg_2Ge_2S_8$ to noncentrosymmetric $(Na_3Rb)Hg_2Ge_2S_8$: mixed alkali metals strategy for infrared nonlinear optical material design, *J. Mater. Chem. C*, 2022, **10**, 3300–3306.

43 G. Kresse and D. Joubert, From ultrasoft pseudopotentials to the projector augmented-wave method, *Phys. Rev. B: Condens. Matter Mater. Phys.*, 1999, **59**, 1758–1775.

44 (*a*) C. Aversa and J. E. Sipe, Nonlinear optical susceptibilities of semiconductors: Results with a length-gauge analysis, *Phys. Rev. B:Condens. Matter Mater. Phys.*, 1995, **52**, 14636; (*b*) S. N. Rashkeev, W. Lambrecht and B. Segall,

Efficient ab initio method for the calculation of frequency-dependent second-order optical response in semiconductors, *Phys. Rev. B: Condens. Matter Mater. Phys.*, 1998, **57**, 3905.
45 D. A. Kleinman, Nonlinear dielectric polarization in optical media, *Phys. Rev.*, 1962, **126**, 1977–1979.
46 CCDC 2488264: Experimental Crystal Structure Determination, 2025, DOI: **10.25505/fiz.icsd.cc2pj7l2**.